Computers and Concrete, Vol. 3, No. 1 (2006) 43-64
DOI: http://dx.doi.org/10.12989/cac.2006.3.1.043

Nonlinear analysis of prestressed concrete structures considering slip behavior of tendons

Hyo-Gyoung Kwak† and Jae-Hong Kim‡

Department of Civil and Environmental Engineering, KAIST, Daejeon 305-701, Korea

Sun-Hoon Kim‡†

Department of Civil and Environmental Engineering, Youngdong University, Chungbuk, 370-701, Korea

(Received March 2, 2005, Accepted January 10, 2006)

Abstract. A tendon model that can effectively be used in finite element analyses of prestressed concrete (PSC) structures with bonded tendons is proposed on the basis of the bond characteristics between a tendon and its surrounding concrete. Since tensile forces between adjacent cracks are transmitted from a tendon to concrete by bond forces, the constitutive law of a bonded tendon stiffened by grouting is different from that of a bare tendon. Accordingly, the apparent yield stress of an embedded tendon is determined from the bond-slip relationship. The definition of the multi-linear average stress-strain relationship is then obtained through a linear interpolation of the stress difference at the post-yielding stage. Unlike in the case of a bonded tendon, on the other hand, a stress increase beyond the effective prestress in an unbonded tendon is not section-dependent but member-dependent. The tendon stress unequivocally represents a uniform distribution along the length when the friction loss is excluded. Thus, using a strain reduction factor, the modified stress-strain curve of an unbonded tendon is derived by successive iterations. The validity of the proposed two tendon models is verified through correlation studies between analytical and experimental results for PSC beams and slabs.

Keywords: tendon; bonded; unbonded; prestressed concrete; nonlinear analysis.

1. Introduction

Prestressed concrete (PSC) is a type of reinforced concrete (RC) in which the steel reinforcement has been tensioned against the concrete. This tensioning operation results in a self-equilibrating system of internal stresses which improves the response of the concrete to external loads. While concrete is strong and ductile in compression, it is weak and brittle in tension, and hence its response to external loads is improved by applying pre-compression. In addition, PSC offers many other advantages such as effective deflection control, delay of cracking, activation of an entire concrete section, lighter weight, and better shear resistance in comparison to RC, and has been widely adopted in long-span bridges, floor slabs, large storage tanks, slender towers, etc.

A great number of finite element analyses for concrete structures have been performed, and many

† Professor, Corresponding Author, E-mail: khg@kaist.ac.kr
‡ PhD Candidate, E-mail: jhongkim@kaist.ac.kr
‡† Professor

numerical models that can simulate the structural response of PSC structures have been followed (Kwak and Fillipou 1990, Kwak and Seo 2002). Moreover, general purpose programs which can analyze the nonlinear behavior of concrete structures have also been developed and popularly used in practice (ADINA 2002, ABAQUS 2003, DIANA 2002). Especially in the numerical analysis of PSC structures, additional attention is given to the modeling of prestressing tendons. For bonded tendons, the deformation field of the tendon is the same as that of concrete on the interface. Therefore, the analysis of PSC members from the initial stage after prestressing transfer to the ultimate loading stage, including relaxation of prestress, shrinkage, and creep of concrete, can be conducted on the basis of the strain compatibility condition and the force equilibrium equation at a section (Kwak and Seo 2002, Kwak and Son 2004).

Since the post-cracking behavior of concrete structures, in which bonded reinforcements such as tendons and/or reinforcing steels are embedded, depends on many influencing factors (the tensile strength of concrete, anchorage length of reinforcements, concrete cover, and steel spacing) that are deeply related to the bond characteristics between concrete and reinforcements, consideration of the tension stiffening effect on the basis of the bond-slip mechanism is absolutely necessary to more exactly evaluate ultimate resisting capacity and load-deformation behavior of concrete structures (Fib 2000).

A wide body of research has been conducted to consider the tension stiffening effect, and many numerical models have also been introduced (CEB 1996). Among these models, consideration of the strain softening branch in the tension region of the stress-strain relation of concrete is one of the generally adopted approaches (Maekawa, *et al.* 2003, Kwak and Kim 2001). Recently, modification of the stress-strain relation of steel has been emphasized, because reaching the yield strength of a bare bar at a cracked section does not necessarily indicate the complete yielding of steel embedded at a cracked element. The average steel stress at a cracked element still maintains an elastic stress rather than the yield strength (Belarbi and Hsu 1994, Kwak and Kim 2004). In spite of these efforts concentrated on the cracking behavior of RC structures, a numerical model that can simulate the tension stiffening effect of PSC structures has not been introduced, primarily because of the different bond characteristics of tendons. Accordingly, to effectively simulate the post-cracking behavior of PSC structures with bonded tendons, a modified stress-strain curve of tendon is introduced in this paper on the basis of the bond mechanism between a tendon and concrete, as was introduced at the reinforcing steel (Fib 2000, Kwak and Kim 2004).

On the other hand, the structural behavior of PSC structures with unbonded tendons is member-dependent instead of section-dependent, and the stress in unbonded tendons depends on the deformation of the entire member and is assumed to be uniform at all sections along the span length. This means that the stress cannot be directly determined from a cross-section analysis with the conventional strain compatibility condition as in the case of bonded tendons. To determine the resisting capacity of PSC structures with unbonded internal tendons, accordingly, an exact prediction of the tendon force must be preceded, and consideration of the slip effect along the tendon sheath as well as the stress relaxation with time is emphasized.

Moreover, the stress-strain curve of the tendon shows a large difference from that of reinforcing steel and is usually described by a multi-linear curve in the numerical analysis of PSC structures (Collins and Mitchell 1991). In advance, a tendon placed in a concrete matrix with an initial profile is approximated by a series of straight segments maintaining a constant force and sectional area (Kwak and Seo 2002). The contribution of the tendon to the element stiffness is computed as though the tendon segment is a steel layer located at a distance calculated by averaging the

eccentricity of the tendon in the case of the discrete model. Meanwhile, in the case of an embedded model, the tendon segment is considered as an axial member built into an isoparametric concrete element such that its displacements are consistent with those of the concrete element (ASCE 1982). The tendon force is also taken into consideration according to the equivalent lateral load concept (Kwak and Seo 2002).

However, these tendon models do not afford ready consideration of the slip and/or bond-slip along the tendon length. In order to consider the interaction between the concrete and tendon, accordingly, a one-dimensional link element, where one end is connected to the tendon node while the other is connected to the concrete, is generally used (ASCE 1982). In addition, a bond-zone element that describes the slip behavior of the contact surface between steel and concrete can also be used (Fib 2000). However, the use of a link element or a bond-zone element in the finite element analysis of PSC structures imposes the following restrictions: (1) the finite element mesh must be arranged in such a way that the tendon is located along the edge of a concrete element; and (2) a double node is required to represent the relative slip between the tendon and concrete. In a complex structure, particularly in three-dimensional models, these requirements lead to a considerable increase in the number of degrees of freedom, not only because of doubling the number of nodes along the tendons but also because the mesh has to be refined so that the bars pass along the edges of concrete elements. The complexity of the mesh definition and the large number of degrees of freedom has discouraged researchers from including the slip effect in many previous studies.

These difficulties in considering the slip effect especially increase in the nonlinear analysis of complex large structures with full modeling of the entire structure using commercialized software such as ADINA (2002), ABAQUS (2003), and DIANA (TNO 2002) because the tendon forces are determined in these programs through a section analysis on the basis of the a perfect bond assumption. Nevertheless, the slip effect must be taken into account in PSC structures with unbonded internal tendons in order to reach to an accurate estimation of the ultimate resisting capacity of the structure. The resisting capacity of a PSC structure with unbonded tendons is surely less than that of a structure with bonded tendons (Collins and Mitchell 1991). Therefore, an improved tendon model, which can consider the slip effect in commercialized software without using any link element that requires double nodes, is introduced in this paper. Instead of utilizing double nodes, sequential iteration and correction procedures are introduced to satisfy the member-dependent properties of the tendon, and the efficiency of the introduced model is verified through a correlation study between experimental data and numerical results. As DIANA 8.1 is used in the nonlinear analysis of PSC structures, more details about the solution procedures can be found elsewhere (TNO 2002).

2. Numerical modeling of tendons

2.1. Bonded tendon

In a cracked cross-section of an RC structure, all tensile forces are balanced by the steel encased in the concrete matrix only. However, between adjacent cracks, tensile forces are transmitted from the steel to the surrounding concrete by bond forces. This effect is called the tension stiffening effect. To verify the bond-slip mechanism, accordingly, many experimental and numerical studies have been conducted (Fib 2000, Kwak and Fillipou 1990). In early studies, the characterization

itself of the tension stiffening effect due to the non-negligible contribution of cracked concrete was the main objective. Recently, following the introduction of nonlinear fracture mechanics in RC theory (ASCE 1982), more advanced analytical approaches have been conducted (CEB 1996), and many numerical models that can implement the tension stiffening effect into the stress-strain relation of concrete have been proposed (Maekawa, *et al.* 2003, Kwak and Kim 2001).

In addition to the use of an average stress-strain relation of concrete that includes the strain softening branch in the tension region, modification of the stress-strain relation for steel must also be accomplished for an accurate assessment of the tension stiffening effect (Kwak and Kim 2004). Reinforcing steel is usually modeled as a linear elastic, linear strain-hardening material with yield strength f_y. However, when reinforcing bars are surrounded by concrete, the average behavior of the stress-strain relation is quite different. The most different feature is the lowering of the yield stress below f_y. Even though the steel stress reaches the yield strength of a bare bar at a cracked section, the average steel stress at a cracked element still maintains an elastic stress less than the yield strength. This is because the concrete matrix located between cracks is still partially capable of resisting tensile forces, owing to the bond between the concrete and reinforcement. Determination of the element stiffness on the basis of the yielding of steel at a cracked section at which a local stress concentration appears in the steel may cause an overestimation of the structural response at the post-yielding range.

Accordingly, to trace the cracking behavior of a RC structure up to the ultimate limit state by using the smeared crack model, in which the local displacement discontinuities at cracks are distributed over some tributary area within the finite element and the behavior of cracked concrete is represented by average stress-strain relations, the average stress-strain relation of steel needs to be defined together with the introduction of the strain softening branch in the stress-strain relation of concrete. Considering these factors, a few modified average stress-strain relations of steel have been proposed and are popularly employed in the numerical analysis of RC structures (Belarbi and Hsu 1994, Kwak and Kim 2004). Nevertheless, direct application of these models into the numerical analysis of PSC structures may not be appropriate because the bond characteristics between tendon and concrete are different from those between reinforcing steel and concrete. Therefore, the average stress-strain relation of a bonded tendon is introduced in this paper on the basis of the bond properties in PSC structures.

The internal tendons incased in a metal sheath are unified with the concrete matrix through grouting. Since the grout material, which consists of a mixture of cement and water (water/cement ratio of about 0.5) together with a water-reducing admixture and an expansive agent, has sufficient strength to bond the tendons to the surrounding concrete, it can be equally considered as concrete while modeling PSC structures with finite elements. On the other hand, the bond characteristics of prestressing tendons present numerous differences with the bond characteristics of reinforcing bars. To define the bond stress-slip relation between a prestressing tendon and grout material, a formula introduced by Balázs (1992) on the basis of experimental studies is used in this paper.

$$f_b(s) = \psi c\sqrt{f_c'}\ (\delta(s))^b = \psi c\sqrt{f_c'}\ (s/d_p)^b \tag{1}$$

where c=2.055 MPa$^{1/2}$, ψ is a constant defining the upper and lower limits of bond stress and has the average value of 1.0, f_c' is the compressive strength of the grout material, d_p is the diameter of the tendon, and b in the range of $0 < b < 1$ represents the tendon type and has a value of 0.25 in the case of seven-wire strands.

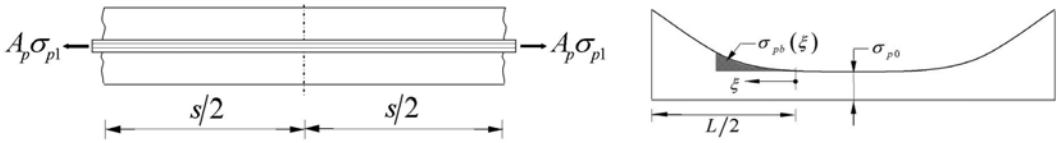

(a) Tension member (b) Stress distribution

Fig. 1 Behavior of tension member

From the strain distribution along the tendon, the local slip $s(x)$ can be defined as the total difference in elongations between the tendon and the concrete matrix measured over the length between a distance x from the separation point between the tendon and the concrete matrix and a crack force in Fig. 1 bounded by two adjacent cracks; that is, $s(x) = \int^x \{\varepsilon_s(t) - \varepsilon_c(t)\} dt$. In advance, on the basis of the force equilibrium, the following very well-known governing differential equation for the bond-slip normalized with respect to d_p can be obtained (Balázs 1992, Kwak and Song 2002).

$$\delta''(\xi) - K_p f_b(\delta(\xi)) = 0 \tag{2}$$

where the normalized slip $\delta(\xi)=s(\xi)/d_p$, $\xi=x/d_p$ is the normalized length from the crack surface, $n=E_p/E_c$, the steel ratio $\rho_p=A_p/A_c$, $K_p=4(1+n\rho_p)\Theta/E_p$, $\Theta=d_p^2\pi/(4A_p)$, and E_p and A_p are Young's modulus and sectional area of the tendon, respectively.

The general solution of Eq. (2) is obtained by applying the boundary condition at the crack face and at the center of the cracked region like the anchorage region of Balázs (1992). After obtaining the general solution for the bond-slip, the corresponding bond stress along the steel axis is successively calculated using the force equilibrium and the compatibility condition at an arbitrary location. Moreover, the tendon stress at an arbitrary location between two adjacent cracks can be inferred from the superposition of the bond stress, transformed to the sectional stress by multiplying 4Θ, on the tendon stress σ_{p0} at the center of the cracked region (see Fig. 1).

$$\begin{aligned}\sigma_p(\xi) &= \sigma_{p0} + 4\Theta\int_0^\xi f_b(\xi)d\xi = \sigma_{p0} + 4\Theta\int_0^\xi \psi c\sqrt{f'_c\sqrt{\delta(\xi)}}d\xi \\ &= \sigma_{p0} + B\xi^{\frac{1+b}{1-b}} = \sigma_{p0} + \left[\frac{4\Theta(1-b)}{1+b}\psi c\sqrt{f'_c}\kappa^b\right]\xi^{\frac{1+b}{1-b}}\end{aligned} \tag{3}$$

The stress distribution of a bonded tendon along the length shows a different shape from that of a reinforcing steel, which is represented by a cosine shape with zero slope at the crack face (Belarbi and Hsu 1994). In addition, in contrast with the bond characteristics in RC members, which show a decrease of bond stress with an increase of slip after reaching the maximum bond stress, the bond stress between tendon and concrete maintains its maximum value up to a larger bond-slip range at the cracked region.

Since the value of $n\rho_p$ is in the range of 0~0.1 and b=0.25 for the seven-wire strands, the variation of $B=(8.47\sim8.74)(f'^2_c/E_p)^{1/3}$ MPa is relatively small, and Eq. (3) can be simplified by using the representative value of B.

$$\sigma_p(\xi) = \sigma_{p0} + 8.5\sqrt[3]{f'^2_c/E_p}\,\xi^{5/3} \tag{4}$$

On the basis of the bond stress distribution at the cracked region in Fig. 1, the bond stress difference between the stress at the crack face and the average stress uniformly distributed within the two adjacent cracks can be calculated by

$$\sigma_{p1}-\sigma_{pa}=\sigma_p\left(\frac{S/2}{d_p}\right)-\frac{d_p}{S/2}\int_0^{\frac{S/2}{d_p}}\sigma_p(\xi)d\xi=7.5\sqrt[3]{f_c'^2/E_p}(S/d_p)^{5/3} \tag{5}$$

Then, the compressive strength f_c' of the grout material can be assumed to be 24 MPa and 55 MPa in the case of pre-tensioned and post-tensioned concrete members, respectively, because the concrete and cement paste act as grout materials in each case (Fib 2000). In addition, experimental data show that the crack space s is in the range of 150 mm~250 mm (Collins and Mitchell 1991). If the average values of s=200 mm and E_p=200,000 MPa are used, Eq. (5) can be simplified by

$$\sigma_{p1}-\sigma_{pa}=\begin{cases}7{,}300/d_p^{5/3} & \text{for pre-tensioning}\\ 12{,}700/d_p^{5/3} & \text{for post-tensioning}\end{cases} \tag{6}$$

where the nominal diameter of tendon d_p and the stress difference $\sigma_{p1}-\sigma_{pa}$ are in mm and MPa, respectively.

On the other hand, the bond stress difference calculated by Eq. (5) or Eq. (6) is based on the assumption that the slip occurs along the entire region from the center of the segment to the crack face. However, when the slip occurs within a limited range, the stress difference will be smaller than that calculated by Eq. (6). This means that the upper limit value for the stress difference needs to be derived. Since the axial force carried by the tendon at the crack face ($A_p\sigma_{p1}$) is equivalent to the axial force along the length ($A_p\sigma_{pa}+A_c\sigma_c$), which is comprised of the average tendon force ($A_p\sigma_{pa}$) and the average concrete tensile force ($A_c\sigma_c$), Eq. (7) can be obtained by using the tension stiffening model of $\sigma_t=f_{cr}(\varepsilon_{cr}/\varepsilon)^{0.4}$, where f_{cr} denotes the tensile strength of the grout material.

$$\sigma_{p1}-\sigma_{pa}=\frac{1}{\rho}\sigma_c=\frac{f_{cr}}{\rho}\left(\frac{\varepsilon_{cr}}{\varepsilon}\right)^4 \tag{7}$$

As mentioned before, the critical difference between bare steel bar and embedded steel bar is in the lowering of yield stress. Even though the yield stress of bare tendon bar is not clearly defined because the prestressing tendon does not exhibit a yield plateau, it can be assumed to be a stress at a strain of 1% (Devalapura and Tadros 1992). Accordingly, Eq. (7) at yielding of tendon can be represented by

$$\sigma_{py}-\sigma_{py}^*=\frac{f_{cr}}{\rho}\left(\frac{f_{cr}/E_c}{0.01}\right)^{0.4}=\frac{6.3}{\rho}\frac{f_{cr}^{1.4}}{E_c^{0.4}} \tag{8}$$

where σ_{py}^* is the apparent yield stress considering the bond characteristics of the embedded tendon bar. This means that the yield stress σ_{py} corresponding to the strain of 0.01 needs to be revised to σ_{py}^*. From Eqs. (6) and (8), the yielding point σ_{py}^* of an embedded tendon bar can finally be calculated by

$$\sigma_{py}^*=\begin{cases}\sigma_{py}-\min[7{,}300/d_p^{5/3},6.3f_{cr}^{1.4}/\rho E_c^{0.4}] & \text{for pre-tensioning}\\ \sigma_{py}-\min[12{,}700/d_p^{5/3},6.3f_{cr}^{1.4}/\rho E_c^{0.4}] & \text{for prost-tensioning}\end{cases} \tag{9}$$

To trace the average stress-strain relation of a tendon generally used in a prestressed concrete structure, the yield stress differences defined in Eq. (9) are calculated and compared in Table 1. The

Table 1 Yield stress differences in tendons

Grouting method	Nominal Diameter of Tendon (d_p)			
	1-strand with 3/8in.	1-strand with 1/2in.	2-strand with 3/8in.	2-strand with 1/2in.
Pre-tensioning	81.1MPa† (170MPa)	81.1MPa† (106MPa)	53.7MPa	33.3MPa
Post-tensioning	81.1MPa† (297MPa)	81.1MPa† (184MPa)	81.1MPa† (93.4MPa)	57.9MPa

† : upper bound of (σ_{py}-σ^*_{py})

tensile strength and Young's modulus of concrete are assumed to be 2.75 MPa and 32,800 MPa, respectively, and the minimum steel ratio of ρ=0.5% is assumed to maximize the yield stress difference. The values in parentheses in Table 1 are determined from the upper boundary values calculated by Eq. (6). As shown in this table, the yield stress differences are gradually governed by Eq. (6) as the nominal diameter of the tendon increases, because this increase accompanies an extension of the bond-slip region at the cracked member.

The yield stress difference in Table 1 has a maximum value of 81.1MPa corresponding to about 5% of the yield strength of the tendon. However, this appears to be relatively small in comparison with that of mild steel, which shows an approximate 25% difference between the yield strength σ_y and apparent yield stress σ^*_y (Belarbi and Hsu 1994). The yield stress difference will also be smaller in real PSC structures where a tendon ratio of more than 0.5% is generally applied. Thus, no remarkable difference in the stress-strain relations of bare tendon and embedded tendon is expected. Accordingly, only slight modification of the stress-strain relation for a bare tendon, rather than deriving a new relation, is sufficient in defining the stress-strain relation of an embedded tendon. Fig.2 shows the modification of the stress-strain relation. Since the linear elastic range is the same as that of the bare tendon, point A in Fig. 2, which represents the upper limit for the linear elastic behavior, can be determined easily from the stress-strain relation of the bare tendon. Point B, representing the apparent yield stress, is then calculated by Eq. (9), followed by determination of point C from the experimental data. In addition, each range bounded by two points (range A to B or B to C in Fig. 2) in a curved line connecting three points of A, B, and C can be simplified with a linear or multi-linear relation.

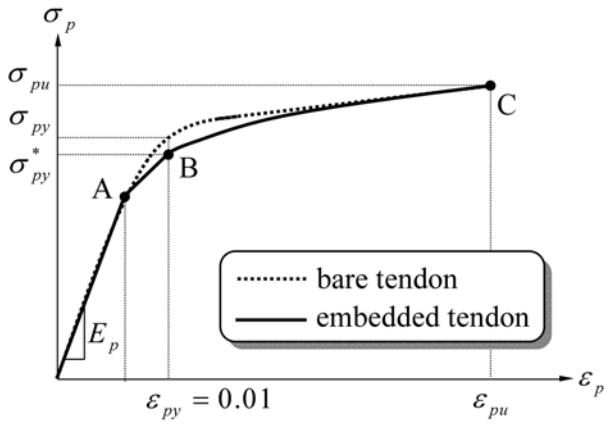

Fig. 2 Simplified average stress-strain relation of embedded tendon

2.2. Unbonded tendon

In contrast with the bonded tendon in which the tension stiffening effect is emphasized, the most dominant effect in the structural response of PSC structures with unbonded tendons is the slip behavior along the tendon sheath. Since the stress increase in the tendons due to external loading is not section-dependent but member-dependent, it cannot be determined from the analysis of a beam cross-section. Rather, it must be determined from the total deformations of the entire structure in the elastic as well as the ultimate limit state. In order to consider the slip in the numerical analysis of a PSC structure with unbonded tendons, accordingly, many analysis methods have been introduced.

Naaman and Alkhairi (1991) proposed a simplified analytical method to determine the strain in a simple beam with a symmetrical tendon profile and subject to symmetrical load. Wu, *et al.* (2001) introduced a friction model that considers friction at the interface of the tendon and concrete using the spring element, and more general analyses of the slip behavior using the finite element method have also been proposed. However, most slip models are based on the spring element that connects the concrete node and the tendon node. As mentioned above, since the spring element in the finite element analysis imposes many restrictions in use, direct application of this element to a large complex structure reinforced with unbonded tendons may be impossible. Accordingly, to take into account the slip effect, an iterative approach is introduced in this paper, instead of taking double nodes as in the case of the spring element, and the calculated slip effect is implemented into the

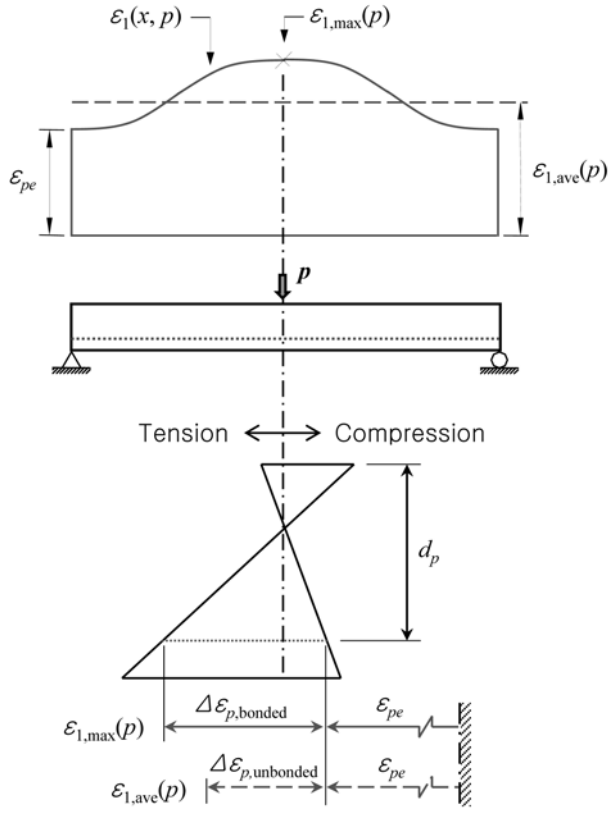

Fig. 3 Strain distribution along length and section

stress-strain relation of the tendon.

First, a PSC structure with unbonded tendons subjected to an external load p is analyzed under the assumption that the tendons maintain bonding with the concrete. If the strain $\varepsilon_1(x, p)$ in Fig. 3 represents the obtained strain distribution along the tendon length in a structure with bonded tendons, then the average strain $\varepsilon_{1,ave}(p)$ and the corresponding average stress $\sigma_{1,ave}(p)$, which are expected to be produced in the same structure with unbonded tendons, can be calculated by Eq. (10).

In addition, the strain value $\varepsilon_{1,max}(p)$ in the strain distribution $\varepsilon_1(x, p)$ may be assumed to be the strain at a critical section in which the maximum stress occurs, and the corresponding point in the stress-strain relation of tendon can be defined by Eq. (11).

$$\varepsilon_{1,ave}(p) = \frac{1}{L}\int_0^L \varepsilon_1(x,p)dx, \quad \sigma_{1,ave}(p) = f(\varepsilon_{1,ave}(p)) \tag{10}$$

$$\varepsilon_{1,max}(p) = \max[\varepsilon_1(x,p)], \quad \sigma_{1,max}(p) = f(\varepsilon_{1,max}(p)) \tag{11}$$

where f represents the stress-strain relation of a bare tendon and L is the total length of a tendon between both anchorages.

As shown in Eqs. (10) and (11), both values of the average strain $\varepsilon_{1,ave}(p)$ and the maximum strain $\varepsilon_{1,max}(p)$ change with the magnitude of the applied load p, which directly affects the tendon force in the prestressing steel. This means that the modified stress-strain relation of embedded tendons, as shown in Fig. 4, is not uniquely defined, but rather it changes in accordance with the applied external load p and the tendon layout along the length in a PSC structure. Accordingly, it is reasonable to construct the modified stress-strain relation of the tendon on the basis of the stress and strain at the critical section, where these represent the maximum values, because all the structural responses from the uncracked elastic to the ultimate limit states are dominantly affected by the structural behavior at this section. Unlike the bonded tendon, which presents the same strain distribution along the length as that of the concrete, the unbonded tendon presents a uniform strain distribution. Therefore, the tendon stress $\sigma_{1,max}(p)$ corresponding to the maximum strain of $\varepsilon_{1,max}(p)$ needs to be revised to the average stress $\sigma_{1,ave}(p)$, because the non-uniform strain distribution with the maximum value of $\varepsilon_{1,max}(p)$ is averaged in the case of an unbonded tendon. That is, as shown in Fig. 4, point A in a bare tendon is moved to point B in an unbonded internal tendon to implement the slip behavior of the tendon. The same modification procedures are repeated for a few different

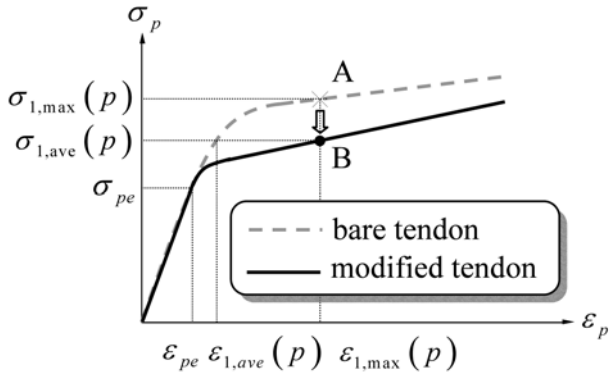

Fig. 4 Modified stress-strain relation of a tendon

load levels to obtain a completely modified stress-strain relation of the tendon defined for the entire stress range.

On the other hand, when a PSC structure with unbonded tendons experiences the crushing failure of concrete before yielding of the tendon, the modified stress-strain relation of the unbonded tendon is only defined up to the strain of the tendon corresponding to the failure of the structure. The following relation is then assumed to be extended to the ultimate state with the same modulus of elasticity determined at the modified stress-strain relation just before the failure of the structure.

Finally, the modified stress-strain relation of g_1 (continuous line in Fig. 4) can be re-defined as

$$g_1^{-1}(\sigma_{1,\text{ave}}(p_i)) = f^{-1}(\sigma_{1,\max}(p_i)) \tag{12}$$

where f is the stress-strain relation of a bare tendon (discontinuous line in Fig. 4), and p_i, where $A_p\sigma_{pe} \le p_i \le A_p\sigma_{pu}$, is the tendon force between the two boundary values of the effective tendon force and the ultimate tendon force.

On the basis of the modified stress-strain relation g_1, a second finite element analysis of the same structure is conducted. Even though the slip effect in the unbonded tendon is indirectly taken into account in the results obtained from the re-analysis, the obtained results must be checked in terms of whether they effectively represent the unbonded characteristics of the tendons. When the results do not reach convergence, re-analyses are repeated on the basis of the revised stress-strain relation, as was the case for the first iteration (see Eq. 13), until the convergence check is satisfied. These steps are presented in greater detail in the flow diagram of Fig. 5.

$$\begin{aligned} g_2^{-1}(\sigma_{2,\text{ave}}(p_i)) &= f^{-1}(\sigma_{2,\max}(p_i)) \\ g_3^{-1}(\sigma_{3,\text{ave}}(p_i)) &= f^{-1}(\sigma_{3,\max}(p_i)) \\ &\vdots \\ g_n^{-1}(\sigma_{n,\text{ave}}(p_i)) &= f^{-1}(\sigma_{n,\max}(p_i)) \end{aligned} \tag{13}$$

Since the maximum tendon stress $\sigma_{j,\max}(p_i)$ experienced at the critical section at each iteration ($1 \le j \le n$) is adjusted to the average value reflecting the characteristics of the unbonded tendon, the convergence can be checked by comparing the two stress components of the maximum tendon stress $\sigma_{j,\max}(p_i)$ obtained from the finite element analysis and the average tendon stress $\sigma_{j,\text{ave}}(p_i)$ corresponding to the average strain from Eq. (10). In this paper, the convergence criterion employed is

$$\frac{\sqrt{\sum_i (\sigma_{j,\max}(p_i) - \sigma_{j,\text{ave}}(p_i))^2}}{\sqrt{\sum_i (\sigma_{j,\text{ave}}(p_i))^2}} \le TOLER \tag{14}$$

where *TOLER* is the specified tolerance and a tolerance of 1%~5% gives a satisfactory convergence.

The slip phenomenon in an unbonded tendon is considered on the basis of the strain compatibility condition modified through implementation of the iteration procedure. By introducing the iteration procedure and extending it to the total strain condition upon the basic concept for the strain reduction coefficient proposed by Naaman and Alkhairi (1991), which defines the ratio of the average concrete strain increment in the unbonded tendon to the strain increment in the equivalent

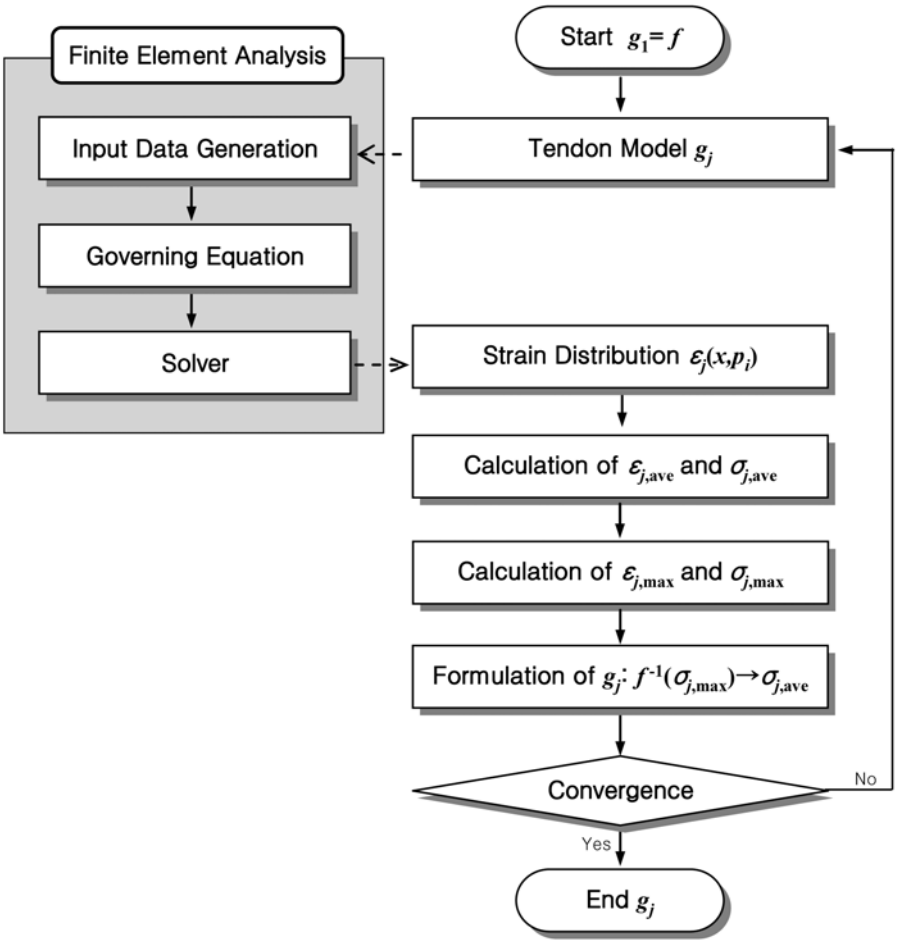

Fig. 5 Flow diagram for construction of modified stress-strain relation of a tendon

bonded tendon at the section of maximum moment in a PSC beam, definition of a modified stress-strain relation for an unbonded tendon becomes possible. In particular, the derivation procedure on the basis of the strain compatibility condition makes it possible to consider the slip behavior indirectly even in the case of modeling an unbonded tendon with embedded and/or distributed steel models. In advance, since any limitation in numerical modeling of a structure to consider the relative slip behavior is not required, the introduced numerical model can effectively be used in the analysis of large complex PSC structures with unbonded tendons using commercialized large programs such as ADINA (2002), ABAQUS (2003), or DIANA (TNO 2002), regardless of the structural type and loading history.

In addition to the slip phenomenon in an unbonded tendon, additional prestressing losses such as friction losses, anchorage slip, and relaxation with time are developed even though the short-term losses occurred at the jacking stage represent relatively small values in the case of unbonded internal tendons and are assumed to be constant after anchorage. Moreover, the tendon force variation by these prestressing losses seems to be very small in comparison with the tendon force

change along the length due to the slip behavior in an unbonded tendon and becomes negligibly small as the applied lateral load increases. Nevertheless, when required, additional consideration for these prestressing losses can be achieved according to the method adopted in classical approaches (Collins and Mitchell 1991) after determining the average stress along the length with the introduced numerical approach. More details related to the numerical implementation of prestressing losses can be found elsewhere (Collins and Mitchell 1991).

3. Solution algorithm

Every nonlinear analysis algorithm consists of four basic steps: the formation of the current stiffness matrix, the solution of the equilibrium equations for the displacement increments, the state determination of all elements in the model, and the convergence check. Ultimately, since construction of the global stiffness matrix and determination of the deformation state of the structure are initiated from the definition of the stress-strain relation of each material, introduction of an accurate stress-strain relation that takes into account many influencing factors is important in simulating the nonlinear behavior of PSC structures. In this regard, the tendon models introduced in this paper can be effectively used. To analyze PSC structures, the DIANA 8.1 general purpose finite element program (TNO 2002) is used, and the other material models including that for concrete are defined according to the CEB-FIP MC90 (1990). In advance, the nonlinear solution scheme selected in this paper uses the tangent stiffness matrix at the beginning of the load step in combination with a constant stiffness matrix during the subsequent correction phase, that is, the incremental-iterative method.

The criterion for measuring the convergence of the iterative solution is based on the accuracy of satisfying the global equilibrium equations or on the accuracy of determining the total displacements. The accuracy of satisfying the global equilibrium equations is controlled by the magnitude of the unbalanced nodal forces. The accuracy of the node displacements depends on the magnitude of the additional displacement increment after each iteration. The latter convergence criterion is used in this study. This can be expressed as

$$\frac{\sqrt{\sum_j (\Delta d_j^i)^2}}{\sqrt{\sum_j (d_j^i)^2}} \le TOLER \tag{15}$$

where the summation extends over all degrees of freedom j, d_j is the displacement of degree of freedom j, Δd_j^i is the corresponding increment after iteration i, and $TOLER$ is the specified tolerance.

In the nonlinear analysis of a RC structure the load step size must be small enough so that unrealistic “numerical cracking” does not take place. These spurious cracks can artificially alter the load transfer path within the structure and result in incorrect modes of failure. Crisfield (1982) has shown that such numerical disturbance of the load transfer path after initiation of cracking can give rise to alternative equilibrium states and thereby lead to false ultimate strength predictions. In order to avoid such problems after crack initiation the load is increased in steps of 2.5%~5.0% of the ultimate load of the member.

The failure load is assumed to occur at a load level for which a large number of iterations is

required for convergence. This means that very large strain increments take place during this step and that equilibrium cannot be satisfied under the applied loads. Obviously the maximum number of iterations depends on the problem and the specified tolerance, but a maximum of 30 iterations seems adequate for a tolerance of 1%. This is the limit in the number of iterations selected in this study.

4. Applications

4.1. PSC beams

To verify the proposed analytical model, two two-span continuous PSC beams with bonded internal tendons are investigated. These beams, A and B, are tested by Lin (1955) to determine the cracking behavior and ultimate strength of PSC beams. The geometry and cross section dimensions of the adopted beams are presented in Fig. 6, and the material properties of concrete reinforcing bar and tendon are summarized in Table 2. The other material properties not mentioned in this paper are determined in accordance with the CEB-FIP MC90 (1990). The prestressing tendon has a concordant profile in this specimen and consists of a straight part, which extends from the end of the beam to the point where the concentrated load is applied, and a curved part over the center support. Moreover, beam B is reinforced with mild reinforcing bars while beam A is not reinforced.

Table 2 Properties of two-span continuous PSC beams

Beam	Concrete		Reinforcing bar		Tendon		
	f_c' [MPa]	f_t [MPa]	A_s [mm^2]	f_y [MPa]	A_p [mm^2]	f_{pe} [MPa]	f_{pu} [MPa]
A	41.30	5.516	-	-	621.3	979.1	1,765
B	41.30	5.516	306.6	313.7	621.3	979.1	1,765

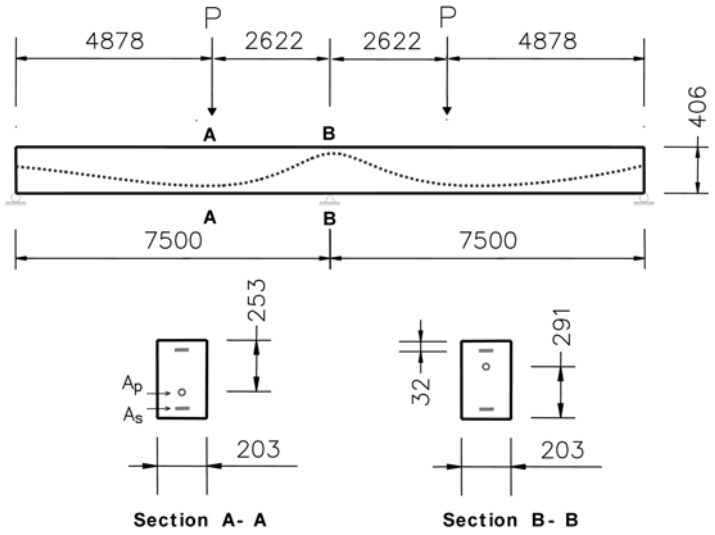

Fig. 6 Configuration of two-span continuous PSC beam (unit: mm)

The concrete was modeled by eight-node serendipity plane stress elements with a 3×3 Gauss integration and the tendon and reinforcements were modeled by an embedded two-node truss element. The number of elements used through the depth and the length of the member are 4 and 150, respectively. Since the plastic hinge length l_p calculated by the simple equation proposed by Sawyer (1964) is determined as 20 cm, the specimen is modeled along the entire span with an element of l=10 cm to obtain an analytical result which is free from the mesh-dependency.

The correlation between the measured load P to the mid-span deflection curves of the two beams and the analytical results is shown in Fig. 7. As shown in this figure, the numerical results obtained by using the modified stress-strain relation of tendon according to the introduced numerical approach and also by considering the tension stiffening effect in concrete give very good agreements with experimental results throughout the entire loading history. On the other hand, the inclusion of only tension stiffening effect produces a slightly overestimation of the ultimate resisting capacity, but the exclusion of tension stiffening effect underestimate the ultimate resisting capacity and gives a soft cracking behavior. It is clear from the comparison of these numerical results with the experimental data that the consideration of tension stiffening effect together with the modification of stress-strain relation of tendon yields a very satisfactory agreement for the structural stiffness and ultimate capacity.

Unlike a beam where the plastic deformation is widely distributed, the plastic deformation in beams A and B subjected to two concentrated load (see Fig. 6), is concentrated at the center support with narrow width, where the occurrence of plastic rotation is initiated and concentrated. This range is called the plastic hinge length. Various empirical expressions have been proposed by investigators for the equivalent length of the plastic hinge l_p (Park and Paulay 1975). Since the structure is modeled with finite elements whose displacement field is defined by the average deformation of nodes, the ultimate capacity can be overestimated if the plastic hinge length is not precisely taken into consideration.

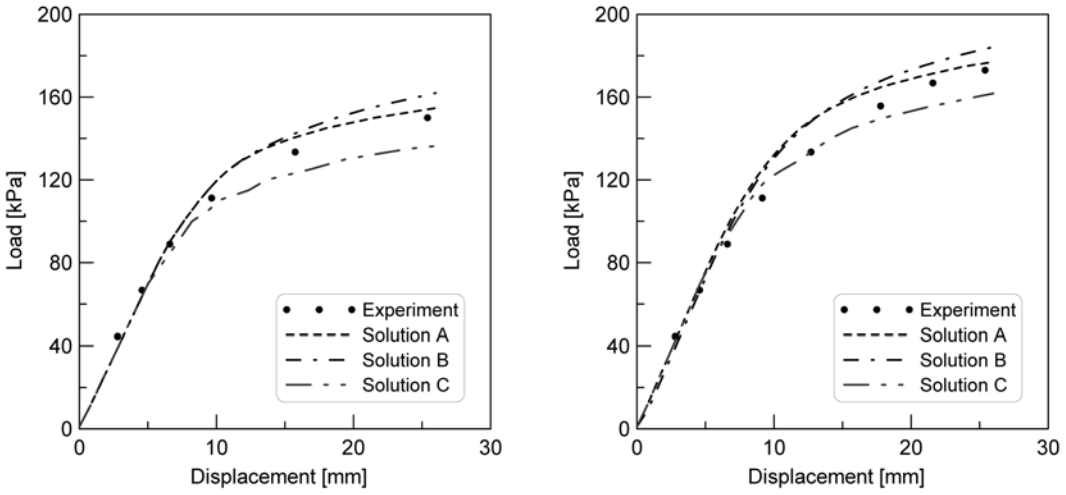

Fig. 7 Comparison of test results and analytical predictions for two-span continuous beam

In order to study the effect of finite element mesh size on the analytical results, accordingly, three different meshes with l=10 cm, l=43 cm, and l=130 cm for the region between the loading point and the center support are investigated. As shown in Fig. 8, the exclusion of plastic hinge length when the element size is greater than the expected plastic hinge length (l_p is about 20 cm in this example structure) may yield an overestimated ultimate load. On the other hand, the numerical results when the element size was 5 cm was exactly the same with those of l=10 cm. Accordingly, three effects of the tension stiffening, modification of stress-strain relation of tendon and plastic hinge length must be considered to reach to a very satisfactory agreement of the model with reality.

In advance, three simply supported PSC beams are also investigated with the same objective of establishing the capacity of the introduced numerical model. The beams, tested by Tao and Du (1985), are specimens A-1 and A-3 with unbonded internal tendons and specimen D-3 with bonded internal tendons. The material properties and geometries of the three test specimens are summarized in Table 3 and Fig. 9, respectively. In advance, the other material properties not mentioned in this paper are determined in accordance with the CEB-FIP MC90 (1990). The same elements with those used in the previous two-span continuous PSC beams were used in modeling the structure, and the number of elements used through the depth and the length of the member are 4 and 26, respectively. Since the concentrated loads are applied at the one-third points of these structures, no additional consideration for the plastic hinge length is required in determining the finite element mesh size (Kwak and Kim 2002) because the plastic deformation is uniformly distributed within the two loading points.

Fig. 10(a) compares the analytical results with the measured load-displacement response of beam D-3, and very satisfactory agreement between analysis and experiment is observed. The analytical results by Chern, *et al.* (1992) are also shown Fig. 10(a). Since Chern, *et al.* used the stress-strain relation of a bare tendon without any modification, the ultimate resisting capacity of the structure was slightly overestimated and the yielding load, after which a large plastic deformation occurs, was not effectively estimated. The comparison of analytical predictions demonstrates the significance of

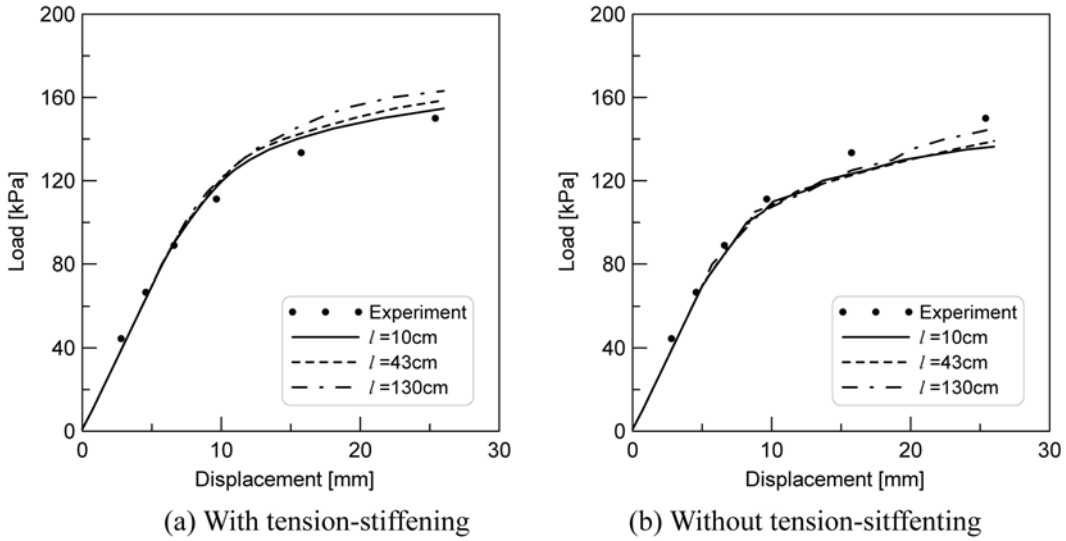

Fig. 8 Mesh size effect in beam A

Table 3 Properties of simply supported PSC beams

Beam	Concrete	Reinforced steel		Tendon			
	f'_c [MPa]	A_s [mm^2]	f_y [MPa]	A_p [mm^2]	f_{pe} [MPa]	f_{py} [MPa]	f_{pu} [MPa]
A-1	30.6	58.8	960	157	267	1,465	1,790
A-3	30.6	156.8	820	236	430	1,465	1,790
D-3	35.6	156.8	879	236	430	1,360	1,660

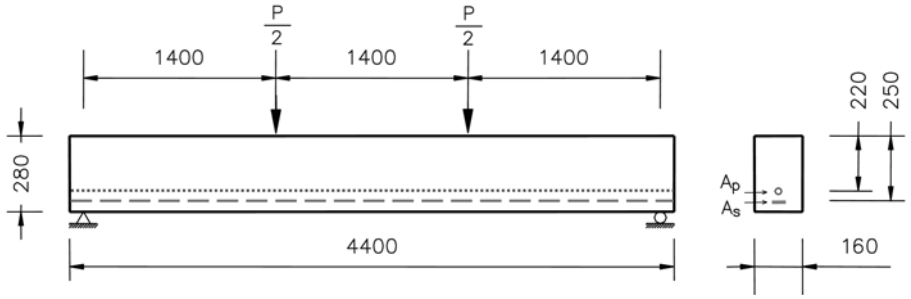

Fig. 9 Configuration of PSC beam (unit: mm)

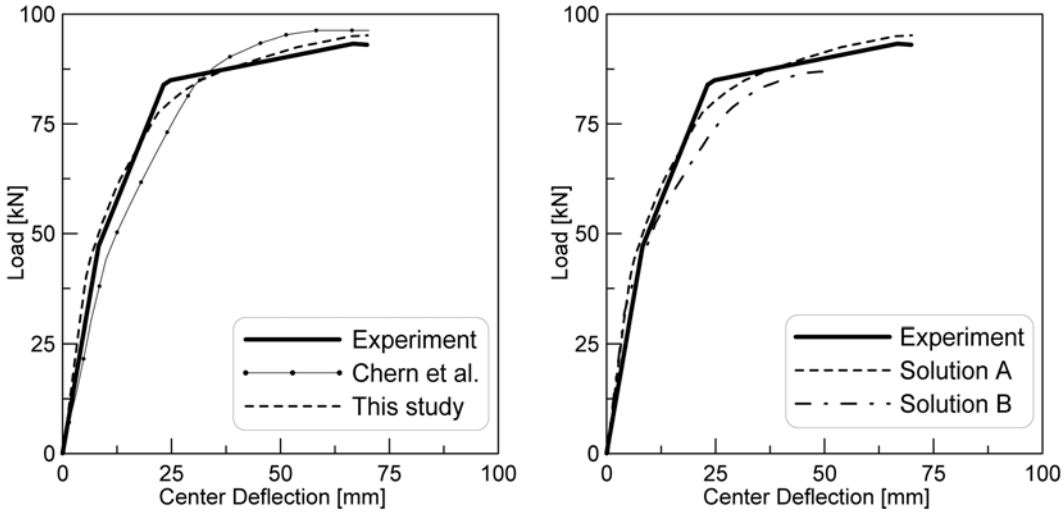

Fig. 10 Numerical results of beam D-3

the modification of the stress-strain relation of the tendon.

To identify the relative contribution of the tension stiffening effect, two different analyses are also performed for this beam. From Fig. 10(b), it is clear that disregarding the tension-stiffening effect yields a slight softer response. These results indicates that the tension-stiffening effect needs to be considered for more accurate prediction of nonlinear responses of PSC structures with bonded

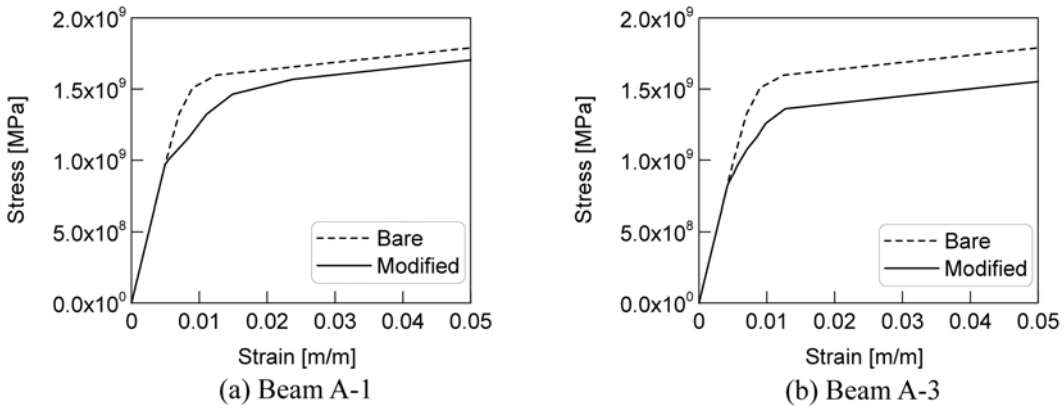

Fig. 11 Modified stress-strain relationship of unbonded tendons

internal tendons, even though the tension stiffening effect induced from the bond mechanism between tendons and surrounding concrete is not relatively dominant.

On the other hand, unlike the case of bonded tendons, analyses of PSC structures with unbonded tendons require the modification of the stress-strain relation of tendon in order to take into account the slip effect. According to the iteration procedure (see Fig. 5), the average stress-strain relation is calculated, and Fig. 12 shows the modified relations for beams A-1 and A-3. Since the difference between the first modification and the second modification was extremely small only two iterations were sufficient at both beam specimens. From Fig. 11 it is inferred that the slip effect will be relatively large in beam A-3 and exclusion of the slip effect will lead to overestimation of the ultimate resisting capacity of PSC structures with unbonded tendons.

The analytical response of beams A-1 and A-3 are compared with the experimental measurements of Tao and Du (1985) and the analytical solutions obtained by Chern, *et al.* (1992) in Fig. 12(a) and Fig. 13(a) respectively. With the effects of tension stiffening and slip, the analyses show excellent agreement with the experimental results, but the exclusion of the slip effect (the numerical results by Chern, *et al.* 1992) leads to overestimation of the ultimate resisting capacity of the PSC beams and relatively stiff behavior after yielding of tendons.

To identify the relative contribution of each effect, four different analyses are performed for these specimens, and the obtained results can be compared in Fig. 12(b) and Fig. 13(b). In contrast with Solution A, which considers both the effects of tension stiffening and slip, Solutions B and D, which exclude the slip effect, produce stiffer responses regardless of consideration of the tension stiffening effect. Moreover, the contribution of slip to the load-displacement responses of the specimens increases with the load.

Comparison of Fig. 10 with Fig. 12 and Fig. 13 leads to the following conclusions. First, the influence of both effects is more dominant in PSC structures with unbonded tendons. Second, exclusion of the tension stiffening effect may lead to underestimation of the ultimate resisting capacity whereas exclusion of the slip effect leads to overestimation. Finally, the numerical analyses of PSC structures with unbonded tendons using commercialized software, composed on the basis of a perfect bond assumption, may lead to incorrect nonlinear responses of structures if additional consideration for the slip effect is not taken into account.

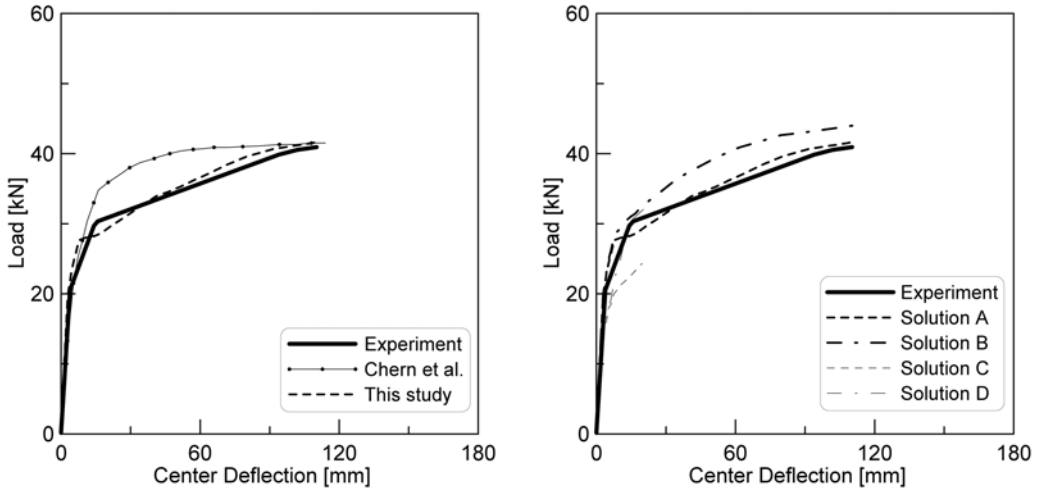

(a) Load-displacement relationship

(b) Tension stiffening and slip effect

Solution A: modified with tension-stiffening
B: bare with tension-stiffening
C: modified without tension-stiffening
D: bare without tension-stiffening

Fig. 12 Numerical results of beam A-1

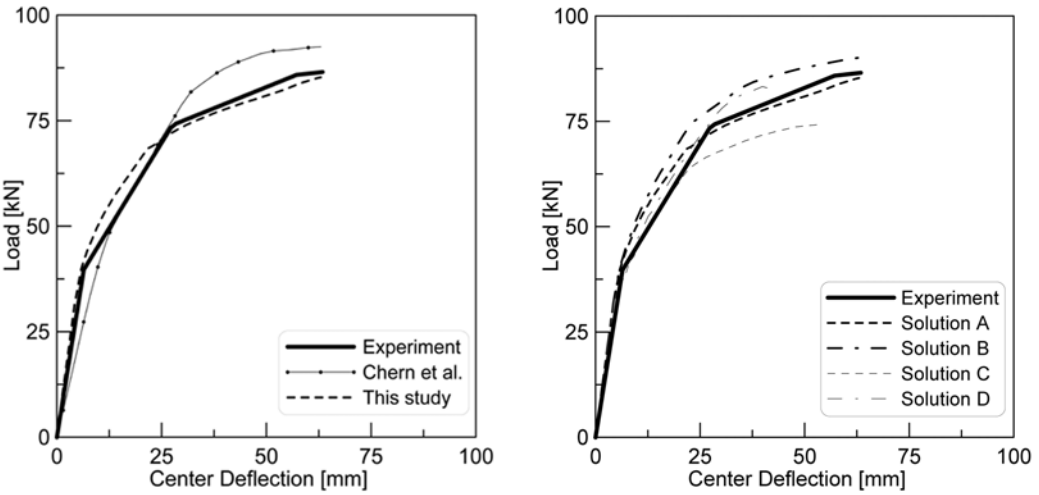

(a) Load-displacement relationship

(b) Tension stiffening and slip effect

Solution A: modified with tension-stiffening
B: bare with tension-stiffening
C: modified without tension-stiffening
D: bare without tension-stiffening

Fig. 13 Numerical results of beam A-3

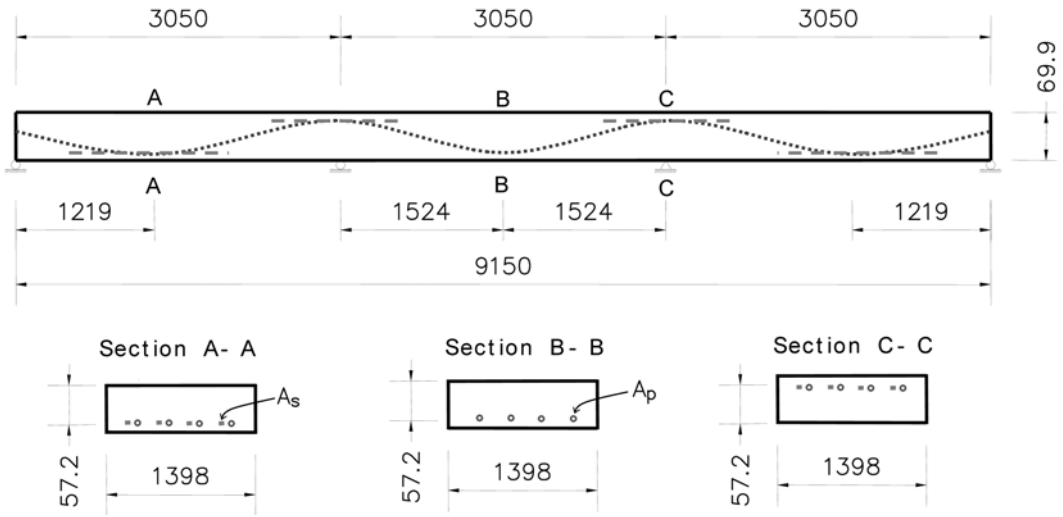

Fig. 14 Geometry of PSC slabs

Table 4 Material properties used in slabs

Concrete	Reinforced steel		Tendon		
f_c' [MPa]	A_s [mm^2]	f_y [MPa]	A_p [mm^2]	f_{pe} [MPa]	f_{pu} [MPa]
32.4	28.3	448	31.68	976	1,655

4.2. PSC slabs

Tension stiffening has a significant effect in the analysis of RC slabs. In order to investigate the validity of the proposed tendon model together with an assessment of the necessity for consideration of the tension stiffening effect, two three-span continuous slabs tested by Burns, *et al.* (1978) are used in the correlation studies. The geometry and cross-section dimensions of the adopted slabs are presented in Fig. 14 and the material properties are summarized in Table 4. The unbonded internal tendons are placed along the total span and mild steels are reinforced at the maximum positive and negative moment regions to prevent abrupt failure and to reserve additional ductility of the structure.

The two slabs are identical except for the loading condition. The first slab, A108, is subjected to a gradually increased live load on the first and third spans under application of a self-weight of w_D=3304 Pa and an additional live load of w_L=1317 Pa on the center span, while the second slab, A109, is subjected to a gradually increased live load on the first and second spans under application of a self-weight of w_D=3304 Pa and an additional live load of w_L=1317 Pa on the third span. A commercialized program, DIANA 8.1 (2002), is used, after defining the stress-strain relations of tendon and concrete on the basis of the introduced tendon model and the strain softening branch of the concrete. Eight-node laminate shell elements are used for the finite element idealization of the slab and 60 elements with 8 imaginary concrete layers through the thickness of the slab are used in the analysis.

Fig. 15(a) and Fig. 16(a) comparing the analytical load-deflection relation at point B with the

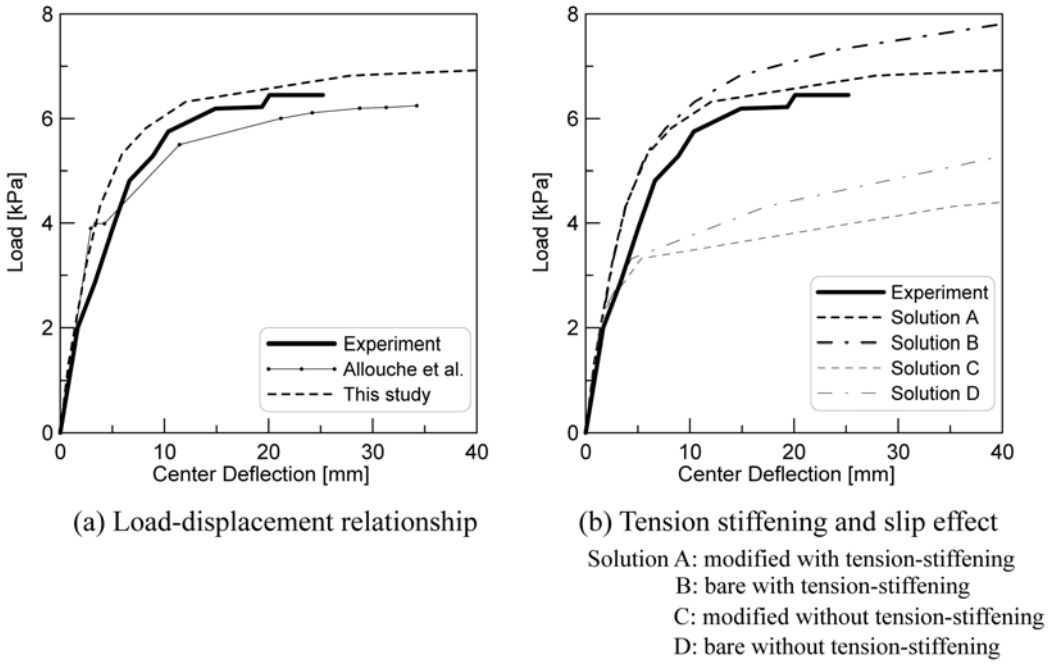

Fig. 15 Numerical results of slab A108

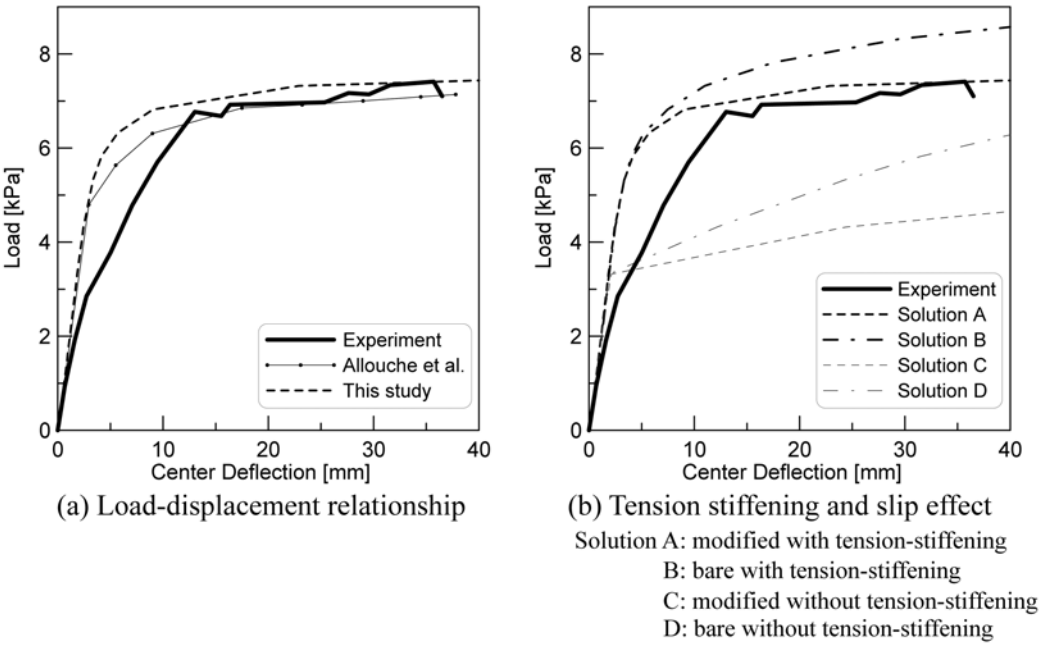

Fig. 16 Numerical results of slab A109

measured experimental data, show that the inclusion of both effects (tension stiffening and slip) yields satisfactory agreement of the model with reality. As shown in these figures, the specimen

cracking behavior may be significantly affected by the loading history. Further, the numerical analyses may have some limitations in tracing the cracking behavior depending on the loading history in shallow bending members, which are dominantly affected by the tension stiffening effect. On the other hand, the live load of w_L=7 kPa closely approximates the ultimate load of the specimens.

In advance, Fig. 15(b) and Fig. 16(b) show that tension stiffening affects the nonlinear behavior of the slab much more than slip, and ignoring the tension stiffening effect clearly leads to underestimation of the ultimate resisting capacity of PSC slabs. Conversely, ignoring the slip effect leads to overestimation of the ultimate resisting capacity of the slabs. The present finding that slip is an important factor in multi-span continuous slabs also agrees with the results of simply supported beams, where the slip behavior along the single curvature is clearly explained. The difference in numerical results between considering and not considering the tension stiffening or slip effect is enlarged with an increase in the applied load.

5. Conclusions

Modified stress-strain relationships of tendon are proposed for the nonlinear finite element analysis of PSC structures with bonded and/or unbonded tendons. The proposed tendon models make it possible to analyze PSC structures using commercialized software such as ADINA, ABAQUS, and DIANA, which are based on a perfect bond assumption. The proposed models do not require a double node to simulate tension stiffening or the slip effect developed at the interface of two adjacent materials of concrete and tendon, and as such they can effectively be used in modeling a large three-dimensional PSC structure. The introduced tendon models have been verified through a comparison of experimental data and numerical results.

Representative PSC beams and slabs were analyzed with the purpose of investigating the relative effects of slip and tension stiffening, and the following conclusions were obtained: (1) the tension stiffening and slip effects are more dominant in a PSC structure with unbonded tendons; (2) ignoring the tension stiffening effect clearly leads to underestimation of the stiffness and ultimate resisting capacity of PSC structures, in contrast with the case of slip effect, and accordingly consistent numerical results for PSC structures can only be obtained when both effects are included in the numerical model; (3) the change in the structural responses according to the use of the modified tendon model in the beam D-3 with bonded tendons is not as large as was found in RC structures with embedded reinforcing steel. This means that the stress-strain relation of a bare tendon can be directly used without any modification for the prediction of the ultimate resisting capacity of a PSC structure reinforced with more than 1.0% steel ration; (4) however, modification of the stress-strain relation of an unbonded tendon must be preceded if no additional slip model is taken into account in the numerical modeling of a PSC structure, regardless of the steel ration, because the slip effect, representing member-dependent behavior, is dominant.

Acknowledgements

The research reported in this paper was made possible by the financial support from the Smart Infra-Structure Technology Center funded by the Korea Science and Engineering Foundation. The authors would like to express their gratitude to this organization for the financial support.

References

ABAQUS, Inc. (2003), *ABAQUS 6.4 Analysis User's Manual*.
ADINA R & D, Inc. (2002), *ADINA Verification Manual.*
Allouche, E. N., Campbell, T. I., Green, M. F., and Soudki, K. A. (1999), "Tendon stress in continuous unbonded prestressed concrete members –Part2: Parametric study", *PCI J.*, January-February, 60-73.
ASCE task committee on finite element analysis of reinforced concrete structures (1982) *State-of-the-Art Report on Finite Element Analysis of Reinforced Concrete.* ASCE.
Balázs, G. L. (1992), "Transfer control of prestressing strands", *PCI J.*, Nov.-Dec., 60-69.
Belarbi, A. and Hsu, T. T. C. (1994), "Constitutive laws of concrete in tension and reinforcing bars stiffened by concrete", *ACI Struct. J.*, **91**(4), 465-474.
Burns, N. H., Charney, F. A., and Vine, W. R. (1978), "Tests of one-way post-tensioned slabs with unbonded tendons", *PCI J.*, Sep.-Oct., 66-81.
Chern, J.-C., You, C.-M., and Bažant, Z. P. (1992), "Deformation of progressively cracking partially prestressed concrete beam", *PCI J.,* Jan.-Feb., 74-85.
Collins, M. P. and Mitchell, D. (1991) *Prestressed Concrete Structures.* Prentice Hall.
Comite Euro-International du Beton (CEB) task group 22 (1996), *RC Elements Under Cyclic Loading*. Thomas Telford.
Comite Euro-International du Beton (CEB) and Federation International de la Prestressing (FIP) (1990) *CEB-FIP Model Code for Concrete Structures.* Thomas Telford.
Crisfield, M. A. (1982), "Accelerated solution techniques and concrete cracking", *Comput. Meth. Appl. Mech. Engng.*, **33**, 587-607.
Devalapura, R. K. and Tadros, M. K. (1992), "Stress-strain modeling of 270ksi low-relaxation prestressing strands", *PCI J.*, Mar.-Apr., 100-106.
Fib Task Group on Bond Models (2000), *Bond of Reinforcement in Concrete.* Federation International du Beton (*fib*).
Kwak, H.-G. and Filippou, F.C. (1990), *Finite Element Analysis of Reinforced Concrete Structures Under Monotonic Loads*. UCB/SEMM-90/14, University of California, Berkeley.
Kwak, H.-G. and Kim, D.-Y. (2001), "Nonlinear analysis of RC shear walls considering tension-stiffening effect", *Comput. Struct.*, **75**(5), 499-517.
Kwak, H.-G. and Kim, D.-Y. (2004), "FE analysis of RC shear walls subject to monotonic loadings", *Magazine Conc. Res.*, **56**(7), 405-418.
Kwak, H.-G. and Kim, S.-P. (2002), "Monotonic moment-curvature relation of RC beams", *Magazine Conc. Res.*, **54**(6), 423-434.
Kwak, H.-G. and Seo, Y.-J. (2002), "Numerical analysis of time-dependent behavior of pre-cast pre-stressed concrete girder bridges", *Constr. Bldg. Mater.,* **16**, 49-63.
Kwak, H.-G. and Son, J.-K. (2004), "Design moment variations in bridges constructed using a balanced cantilever method", *Constr. Bldg. Mater.*, **18**, 753-766.
Kwak, H.-G. and Song, J.-Y. (2002), "Cracking analysis of RC members using polynomial strain distribution function", *Eng. Struct.*, **24**(4), 455-468
Lin, T. Y. (1955), "Strength of continuous prestressed concrete beams under static and repeated loads", *ACI J.*, **26**(10), 1037-1059.
Maekawa, K., Pimanmas, A., and Okamura, H. (2003), *Nonlinear Mechanics of Reinforced Concrete.* Spon Press.
Naaman, A. E. and Alkhairi, F. M. (1991),"Stress at ultimate in unbonded post-tensioning tendons: Part 2 – Proposed methodology", *ACI Struct. J.*, **88**(6), 683-692.
Park, R. and Paulay, T. (1975), *Reinforced Concrete Structure*, John Wiley & Sons.
Sawyer, H. A. (1964), "Design of concrete frames for two failure states", *Proceedings of the International Symposium on the Flexural Mechanics of Reinforced Concrete*, ASCE-ACI, Miami, 405-431
Tao, X. and Du, G. (1985), "Ultimate stress of unbonded tendons in partially prestressed concrete beams", *PCI J.*, Nov.-Dec., 72-91.
TNO Building and Construction Research (2002), *DIANA-8.1 User's Manual.*
Wu, X. H., Otani, S., and Shiohara, H. (2001), "Tendon model for nonlinear analysis of prestressed concrete structures", *J. Struct. Eng.*, ASCE, **127**(4), 398-405.

CC